Journal of the European Ceramic Society 38 (2018) 2027–2034

Contents lists available at ScienceDirect

Journal of the European Ceramic Society

journal homepage: www.elsevier.com/locate/jeurceramsoc

Original article

A versatile approach for the preparation of ceramics with porosity gradient: by using manganese and tin oxides as a model

Júlio César Sczancoski[a,*], Edson Roberto Leite[a,b]

[a] Universidade Federal de São Carlos (UFSCar), Department of Chemistry, São Carlos, SP, Brazil
[b] Brazilian Nanotechnology National Laboratory (LNNano), CNPEM, Campinas, SP, Brazil

ARTICLE INFO

Keywords:
Porous ceramics
Sintering
Tin compounds
Densification
Porosity gradient

ABSTRACT

Porous ceramics that exhibit porosity gradient are considered promising materials from the industrial point of view, especially for the production of ceramic membranes and filters. This paper describes a simple and versatile approach to produce ceramics with porosity gradient. In order to perform this study, MnO_2/SnO_2 bi-layered pellets were conformed via uniaxial pressure and sintered at 1100 °C and 1300 °C for different times. MnO_2 layer had the role of sintering aid, while the SnO_2 layer was chosen as ceramic matrix subjected to the densification. The field emission scanning electron microscope (FE-SEM) was employed to obtain information on the microstructural features of these pellets. FE-SEM micrographs revealed that the overall percentage of porosity, pore size and shape in SnO_2 layer can be controlled by sintering variables (temperature and time). The results indicated a correlation between the porosity gradient in SnO_2 with the Mn concentration gradient in this matrix.

1. Introduction

In the last years, advanced porous ceramics (PCs) have been widely investigated by the scientific community because they exhibit unique and special features in relation to their dense bulk, as a consequence of their designed porous structure, including overall percentage of porosity, pore size and shape, pore size distribution, porosity gradient and microstructure [1,2]. In general, these kinds of ceramics have a great potential for technological applications involving wear, corrosive media and high operating temperatures [3]. Some examples of commercial applications include ceramic membranes and filters for gas separation or liquid waste pretreatment [4–6], biomaterials for hard tissue repair [7,8], electrodes for solid oxide fuel cells [9,10], reactors for catalytic reactions [11,12], high-temperature insulating refractories [13], pyroelectric material for infrared detectors and thermal imaging devices [14–16], and so on.

The preparation route is one of the key parameters that directly influence the porosity and final physicochemical properties of ceramic oxides. The most traditional experimental methods employed for the preparation of PCs are powder pressing [17,18], slip-casting [19,20], centrifugal casting [21,22], sol-gel route [23,24], freeze casting [25,26], foam techniques [27,28], extrusion [29,30], and so on. Despite the wide variety, there is still an enormous interest from researchers in new processing approaches able to offer an efficient control on the composition, microstructure and porosity of materials as well as operational advantages of low cost, environmentally friendly and easy handling.

Thus, in the present study, a simple and versatile approach for the preparation of ceramics with porosity gradient was proposed in detail. This approach is based on the conformation of ceramic powders as bi-layered pellets by means of uniaxial pressure with posterior sintering. In these pellets, the top layer is composed of any material with features of sintering aid, while the bottom layer is formed by a desired ceramic matrix subjected to densification process. The mass transport and densification mechanisms in these samples are governed by both time and temperature conditions during sintering. For our specific case, the sintering is a phenomenon thermodynamically activated and controlled by the grain-boundary [31]. Hence, monitoring the time and temperature, the atomic mobility of species adopted as sintering aid can be controlled in the ceramic material.

An interesting material to demonstrate the potential of our experimental approach is the tin oxide (SnO_2). Particularly, SnO_2 was taking into account in this study because of its numerous technological applications reported in the literature (for example, gas sensors [32], electrode dye-sensitized in solar cells [33], catalysts [34], varistors [35], and electrodes for lithium batteries [36]) as well as due to the difficulty in sintering a dense bulk of this semiconductor oxide. The fundamental reason responsible for this behavior is explained by the predominance of non-densifying mechanisms (surface diffusion and evaporation-condensation) actuating on the mass transport between

* Corresponding author.
E-mail address: jcsfisica@gmail.com (J.C. Sczancoski).

http://dx.doi.org/10.1016/j.jeurceramsoc.2017.10.028
Received 16 September 2017; Received in revised form 10 October 2017; Accepted 15 October 2017
Available online 16 October 2017

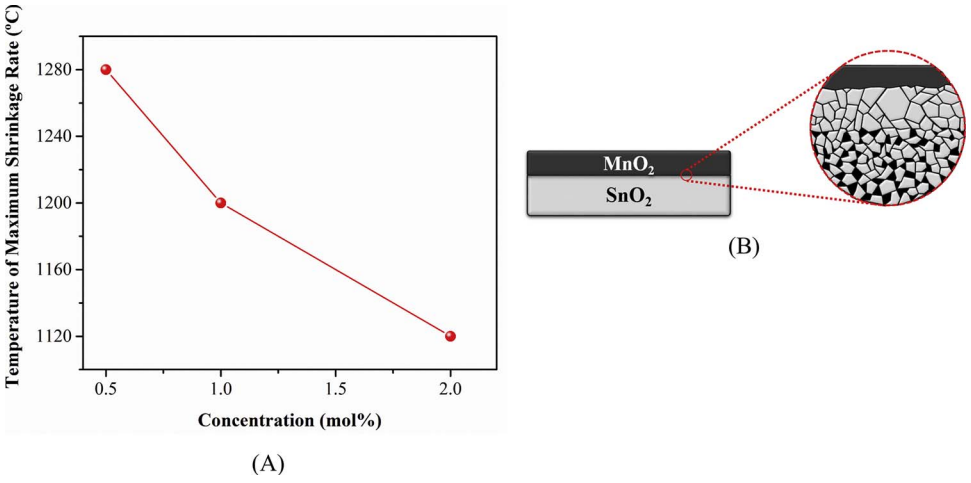

Fig. 1. (A) Temperature of maximum shrinkage rate of SnO_2 as a function of the concentration (mol%) of MnO_2 (experimental data based on Ref. [39]); (B) schematic representation of MnO_2/SnO_2 bi-layered pellets illustrating the formation of the porous structure with porosity gradient.

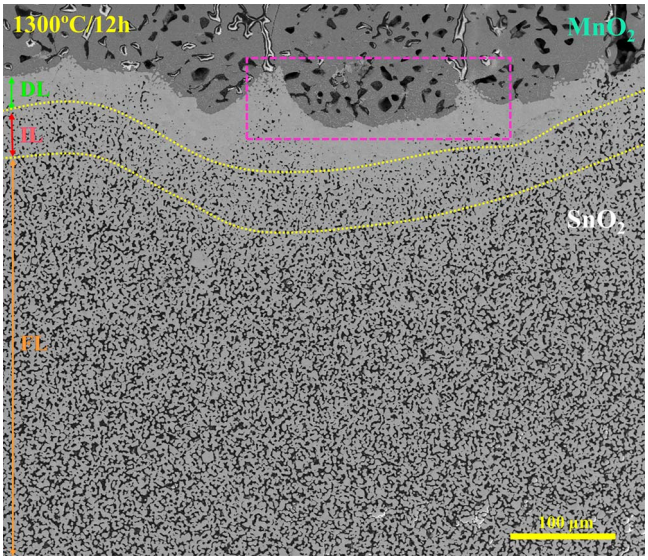

Fig. 2. FE-SEM micrograph showing a typical porous structure of MnO_2/SnO_2 bi-layered pellets sintered at 1300 °C for 12 h. Three regions with different porosities were identified, which were referred as dense layer (DL), intermediary layer (IL) and final layer (FL), respectively. The magenta rectangle denotes the curvature caused by the conformation of MnO_2 and SnO_2 powders as bi-layered pellets via uniaxial pressure with posterior sintering. (For interpretation of the references to colour in the text, the reader is referred to the web version of this article.)

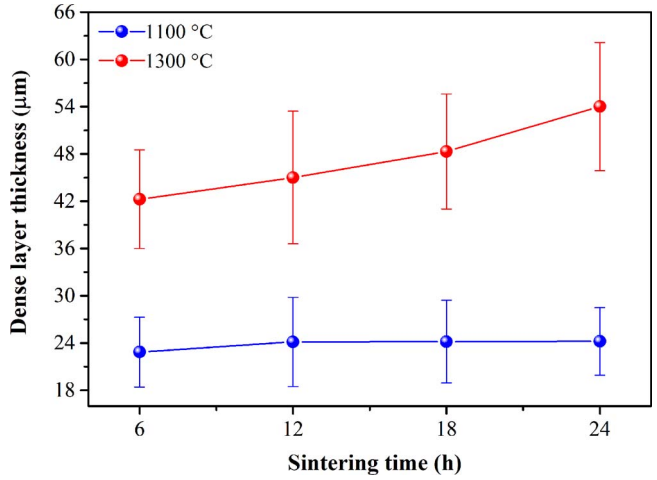

Fig. 3. Dense layer thickness as a function of sintering time for MnO_2/SnO_2 bi-layered pellets sintered at 1100 °C and 1300 °C, respectively.

SnO_2 particles, which promote the coarsening and grain growth [37,38].

The insight to develop our approach was based on the pioneering study performed by Cerri et al. [39]. These authors verified a significant decreasing in the temperature of maximum shrinkage rate for SnO_2 when the MnO_2 content was increased (Fig. 1(A)). These authors established an important correlation between the densification of SnO_2 with the concentration gradient of MnO_2.

Having seen the impact of this research previously published and considering our proposed approach, MnO_2/SnO_2 bi-layered pellets were conformed to induce the formation of a porosity gradient in SnO_2 matrix via diffusion of Mn species (sintering aid) (Fig. 1(B)). The sintering temperatures were selected close to the maximum shrinkage rate of SnO_2 [39], i.e., 1000 °C and 1300 °C, respectively. The sintering kinetics was monitored considering the times of 6 h, 12 h, 18 h, and 24 h.

2. Experimental procedure

2.1. Sample preparation

High purity commercial tin (IV) oxide (≥99% purity, Merck) and manganese (IV) oxide (≥99%, Sigma-Aldrich) were used as raw materials to prepare the sintered bi-layered pellets. Firstly, using a stainless steel punch and die set, 0.750 g of SnO_2 and 0.375 g of MnO_2 were uniaxially pressed at 55 MPa for 35 s. The bi-layered pellets were formed with dimensions of 1.3 cm (diameter) and 0.264 cm (thickness), resulting in a green density of approximately 3.2 g/cm^3. Binders or additives were not added in dried and compacted powders. The obtained pellets were sintered under air atmosphere in a box-type furnace (Lindberg/Blue M, Thermo Scientific, USA) at 1000 °C and 1300 °C for different times (6 h, 12 h, 18 h, and 24 h), maintaining a constant heating rate of 10 °C/min.

In the sequence, the bi-layered pellets were embedded in epoxy resin (Epoxicure Resin and Epoxicure Hardener, Buhler Ltd., USA), which were posteriorly cut in half with a diamond wafer blade by using an ISOMET precision cutter (Buhler Ltd., USA). For a better microstructural investigation, all pellets were subjected to several steps of polishing. Basically, it was used the polishing with 1200 grit SiC sandpaper (Norton, Brazil), diamond paste (mean grit size of 1 μm) in an Aropol-2 v Grinder-Polisher (Arotec, Brazil), and alumina (mean grit size of 0.3 μm) in a VibroMet2 polisher (Buhler Ltd., USA), respectively. Finally, the polished samples were placed in glass beakers containing isopropyl alcohol (99,8% Tedia) and cleaned in an ultrasonic bath (model 1510, Branson, USA) for 30 min.

It is important to emphasize that MnO_2 layer was not removed in the final pellets in order to show its importance for the formation of a porosity gradient in SnO_2. In principle, this MnO_2 layer can be

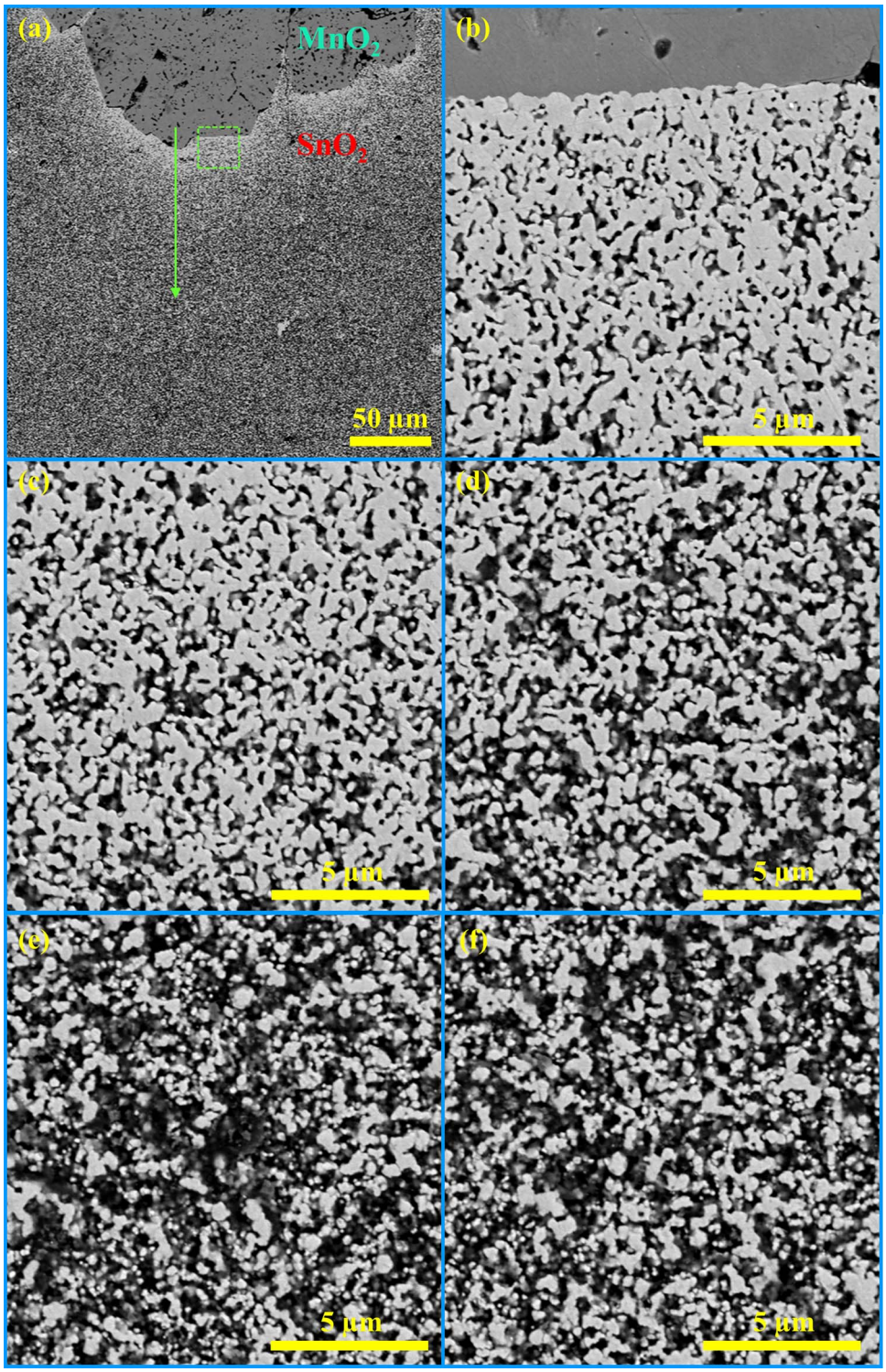

Fig. 4. FE-SEM micrographs of cross-section profiles of MnO_2/SnO_2 bi-layered pellets sintered at 1100 °C for 6 h. The small dotted green square and green arrow (a) indicate the initial region and direction in which the other high magnification micrographs were obtained (from (b) to (f)). (For interpretation of the references to colour in this figure legend, the reader is referred to the web version of this article.)

chemically removed by using a diluted hydrochloric acid solution, without affecting the SnO_2.

2.2. Microstructural characterization

The final microstructure of each sintered bi-layered pellet was minutely investigated on a field emission gun scanning electron microscopy (FE-SEM) (FEI, Netherlands). This analysis was performed by using a beam deceleration of 5 kV, spot size of 3.0, and a low-kV high contrast detector.

2.3. Average pore area

A more quantitative analysis on the average pore area of ceramic pellets was quantified with the *Image J* software [40], according to the procedure described in Ref. [41]. The counting of approximately twenty micrographs of each sample was necessary in order to estimate the porosity gradient with higher statistical reliability. As can be seen in Fig. 2, three regions with different degrees of porosity were identified by means of cross-section profiles of sintered pellets, which were referred as dense layer (DL), intermediary layer (IL) and final layer (FL),

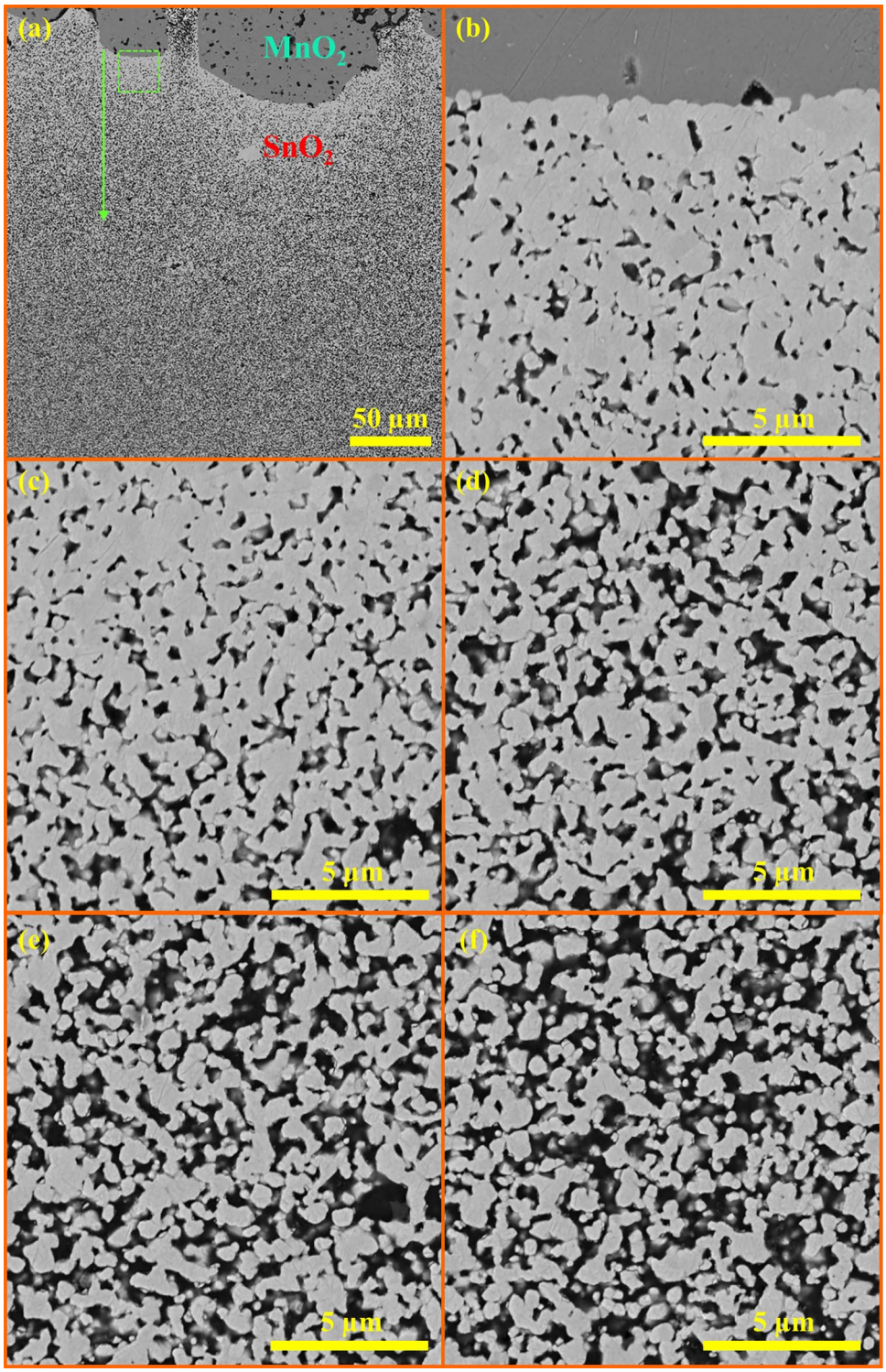

Fig. 5. FE-SEM micrographs of cross-section profiles of MnO_2/SnO_2 bi-layered pellets sintered at 1100 °C for 24 h. The small dotted green square and green arrow (a) indicate the initial region and direction in which the other high magnification micrographs were obtained (from (b) to (f)). (For interpretation of the references to colour in this figure legend, the reader is referred to the web version of this article.)

respectively. The interface region between the MnO_2 and SnO_2 layers is not flat, presenting a curvature caused by the conformation of the powders, when subjected to the uniaxial pressure with posterior sintering process (magenta rectangle in Fig. 2). Thus, this curvature phenomenon does not come from the densification mismatch between these different oxides during sintering.

3. Results and discussion

3.1. Dense layer analysis

In general, the presence of a fully DL in PCs is an essential criterion for specific commercial purposes involving mechanical strength and/or filtration. For example, in ceramic tiles, the formation of a denser surface layer is able to improve the mechanical strength by approximately 30%, when compared to others formed by an entirely porous matrix [1]. In ceramic membranes or filters employed for gas

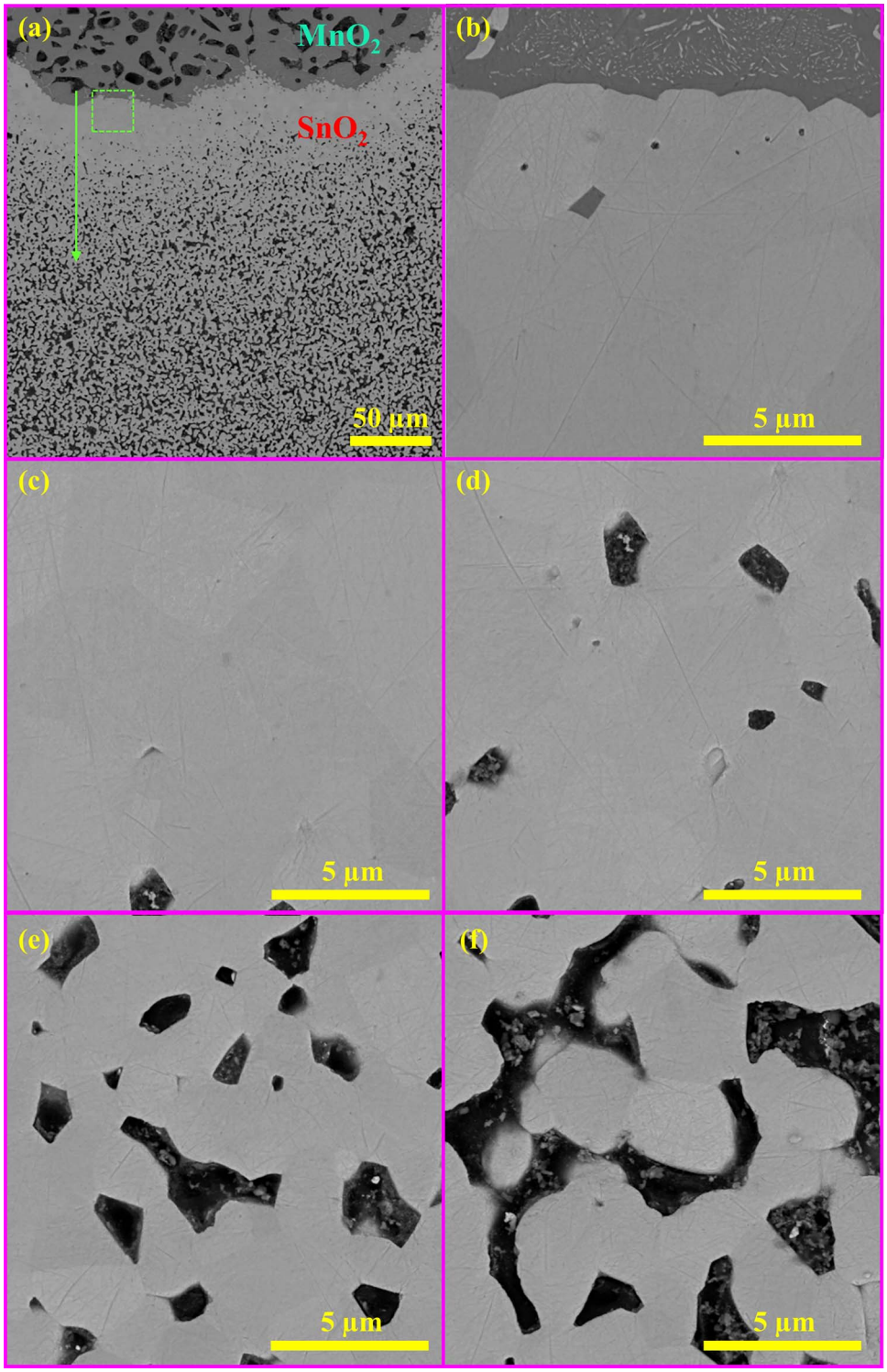

Fig. 6. FE-SEM micrographs of cross-section profiles of MnO_2/SnO_2 bi-layered pellets sintered at 1300 °C for 6 h. The small dotted green square and green arrow (a) indicate the initial region and direction in which the other high magnification micrographs were obtained (from (b) to (f)). (For interpretation of the references to colour in this figure legend, the reader is referred to the web version of this article.)

separation, DL has an important role in blocking the direct passage of specific species in a gaseous mixture (as thin barriers), so that only ions of one type of gas selectively migrate through the membrane [5,6,42,43].

Fig. 3 shows the DL thickness as a function of sintering time for MnO_2/SnO_2 bi-layered pellets sintered at 1100 °C and 1300 °C, respectively. Once pellets are subjected to sufficiently high temperatures, the sintering promotes a strengthening of the microstructure (neck growth between particles), densification (removal of porosity accompanied by shrinkage), and coarsening (grain growth and/or pore growth) [44]. In a previous analysis on the obtained results, the pellets sintered at 1100 °C did not reveal significant changes in their DL thickness with the evolution of time, maintaining a constant value at around 23 µm. In contrast, there is a progressive increase in this layer when the sintering temperature was maintained at 1300 °C, resulting in a maximum thickness of 54 µm after 24 h.

Initially, comparing these results, the diffusion is not sufficiently high for the temperature of 1100 °C, which induces a slower mobility of Mn ions into the SnO_2 layer. Assuming that the diffusion of Mn ions occurs via grain boundary, this transport phenomenon will be

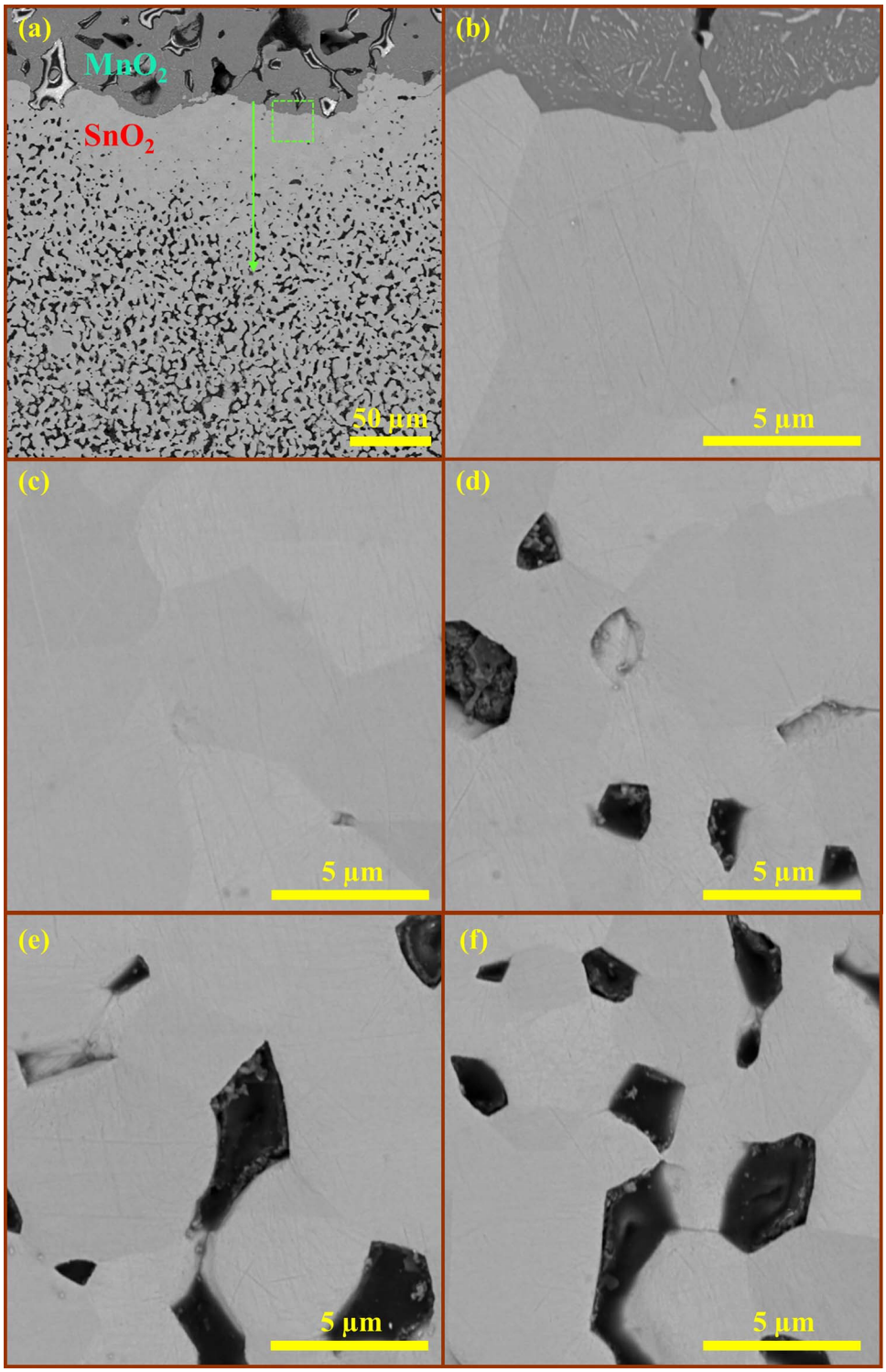

Fig. 7. FE-SEM micrographs of cross-section profiles of MnO_2/SnO_2 bi-layered pellets sintered at 1300 °C for 24 h. The small dotted green square and green arrow (a) indicate the initial region and direction in which the other high magnification micrographs were obtained (from (b) to (f)). (For interpretation of the references to colour in this figure legend, the reader is referred to the web version of this article.)

minimized by the reducing the total area of grain boundary (grain growth process). On the other hand, the sintering temperature of 1300 °C provided a driving force to diffuse the Mn ions to deeper regions along the SnO_2 layer (before the grain and pore stabilization stages), causing a significant increase of DL thickness. All these preliminary results revealed that in our proposed approach, both temperature and time play a decisive role on the matter transport kinetics, especially on the final DL thickness of the ceramic body with porosity gradient.

3.2. Microstructural profiles

Figs. 4–7 illustrate typical FE-SEM micrographs of cross-section profiles of MnO_2/SnO_2 bi-layered pellets sintered at 1100 °C and 1300 °C for 6 h and 24 h, respectively. The micrographs of other pellets with different sintering times, but under the same temperature conditions are displayed in Supplementary Data (SD). In these micrographs, there is a clear difference in microstructural features and degree of porosity in each pellet, as a consequence of both sintering variables, temperature and time. Firstly, analyzing only the pellets sintered at

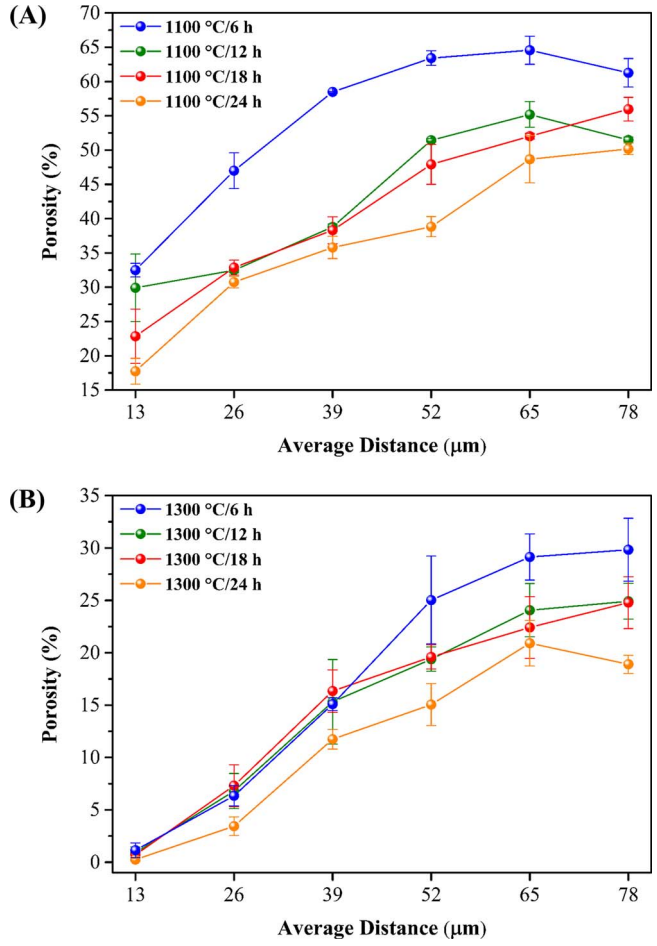

Fig. 8. Porosity as a function of average distance from the interface in MnO_2/SnO_2 bi-layered pellets sintered at 1100 °C (A) and 1300 °C (B) for different times, respectively. (For interpretation of the references to colour in the text, the reader is referred to the web version of this article.)

1100 °C, the polycrystalline microstructure is composed of irregular and elongated grains, containing a high concentration of interconnected pores (open pores) [45]. Another important point to be considered is the gradual increase in porosity from top to bottom into the SnO_2 layer, i.e., a porous structure containing a porosity gradient (Figs. 4, 5, S1 and S2 in SD). Therefore, we believe that there is a transport of Mn ions toward the SnO_2 layer. As this diffusion mechanism is not uniform over the entire SnO_2 layer, a porosity gradient is formed in this layer because it contains different levels of Mn locally situated in the grain boundary, resulting in distinct densification rates. Thus, the regions of SnO_2 with high concentrations of Mn presented an improvement in densification.

On the other hand, maintaining the same temperature of 1100 °C, but extending the sintering time from 6 h to 24 h (Figs. 4, 5, S1 and S2 in SD), the micrographs revealed that the pellets presented an increase in the degree of densification. This result confirms that the time evolution was enough to induce the transport of Mn species to deeper regions into the SnO_2 layer.

For bi-layered pellets sintered at 1300 °C, but maintaining the same sintering times (from 6 h to 24 h), it was evidenced a high-density microstructure (especially close to the MnO_2/SnO_2 interface), containing a lower pore fraction (open and closed porous) with larger grains (Figs. 6, 7, S3 and S4 in SD). In these micrographs, the slight grain orientation contrast detected in the SnO_2 layer is caused by the superficial electron channeling energy [46]. As expected, there is a porosity gradient along the SnO_2 layer (as move away from the MnO_2/SnO_2 interface), which is directly related to the presence of a gradient concentration of Mn species. Thus, the areas in SnO_2 layer with high Mn content presented a significant improvement in the densification. It is important to point out that the increase of temperature was a very important condition to promote an increase in the diffusion rate as well as in the concentration of these Mn species into the SnO_2. Hence, DL thickness exhibited a pronounced increase with similar microestrutural features to a dense bulk (Figs. 6 (a), 7 (a)). Analogously, DL acts as a "valve", which is able to allow the flow of Mn ions into the SnO_2 layer (as an open valve) during the densification stages. However, after its complete densification, the continuous migration of Mn ions towards the SnO_2 (via interface region) is interrupted (as a closed valve). Due to this behavior, the concentration of Mn ions is not enough to yield a fully dense SnO_2 body, even in sintering conditions performed at high temperatures and long times.

3.3. Porosity

Porosity as a function of average distance in MnO_2/SnO_2 bi-layered pellets (Figs. 8 , S5 and S6 in SD) was estimated in order to corroborate with our previous results. It is important to point out that the porosity was calculated along the cross-section profile of each pellet, considering the MnO_2/SnO_2 interface as initial point. In these figures, the curve profiles are very similar, i.e., there is a significant increase in the porosity when moving away from the interface region. This typical behavior characterizes the predominance of a porosity gradient, which is arising from a concentration gradient of Mn species in SnO_2. For sintering performed at 1100 °C (Figs. 8 (A) and S5 in SD), there is a slight reduction in porosity as a function of average distance, when the processing time was increased. Therefore, depending on the sintered pellet, the porosity close to the interface is approximately 17%–35% (13 μm–26 μm) (DL and IL), while the maximum ranges from 50% to 65% (65 μm–78 μm) (FL). On the other hand, for pellets sintered at 1300 °C (Figs. 8 (B) and S6 in SD), also was observed a reduction of porosity with the distance; however, the maximum values were obtained at levels within the range 17%–30% (65 μm–78 μm) (FL). This evidence implies in a great importance of temperature to control the porosity level into the SnO_2 layer. From a kinetics viewpoint, the temperature favors the transport of Mn species to consolidate the densification of SnO_2 in the sintering. Hence, in order to obtain the minimum of porosity, it is necessary high temperatures and long processing times to promote the reduction or elimination of pores during the densification stages.

Taking into account all results above mentioned, we presume that our proposed approach analyzed for MnO_2/SnO_2 bi-layered pellets has a great potential to be employed in other ceramic systems that require the use of effective sintering aids to assist in their densification, such as silicon nitride [47], silicon carbide [48], boron carbide [49], aluminum nitride [50], and so on.

4. Conclusions

In summary, we demonstrate a versatile approach to achieve ceramic solids with the presence of porosity gradient. By controlling the sintering variables (temperature and time), it was possible to modify the porosity level in SnO_2 layer. In principle, both temperature and time are able to control the diffusibility of Mn ions along the SnO_2 layer. A significant reduction in the overall percentage of porous in SnO_2 layer was observed when the sintering was performed at 1300 °C for 24 h. The areas containing high concentrations of Mn species were responsible for the improvement in densification of SnO_2, especially close to the MnO_2/SnO_2 interface.

Conflicts of interest

None.

Acknowledgements

The authors are grateful to FAPESP (CEPID – 2013/07296-2), CAPES (PNPD – 20131475) and CNPq for the financial support.

Appendix A. Supplementary data

Supplementary data associated with this article can be found, in the online version, at http://dx.doi.org/10.1016/j.jeurceramsoc.2017.10.028.

References

[1] A. Shimamura, M. Fukushima, M. Hotta, T. Ohji, N. Kondo, Fabrication and characterization of porous alumina with denser surface layer by direct foaming, J. Ceram. Soc. Jpn. 125 (1) (2017) 7–11.
[2] B. Dong, G. Wang, B. Yuan, J. Han, K. Chen, H. Li, Fabrication and properties of porous alumina ceramics with three different pore sizes, J. Porous Mater. (2016).
[3] A.R. Studart, U.T. Gonzenbach, E. Tervoort, L.J. Gauckler, Processing routes to macroporous ceramics: a review, J. Am. Ceram. Soc. 89 (6) (2006) 1771–1789.
[4] P. Wu, Y. Xu, Z. Huang, J. Zhang, A review of preparation techniques of porous ceramic membranes, J. Ceram. Process. Res. 16 (1) (2015) 102–106.
[5] S.K. Kamarudin, W.R.W. Daud, A.W. Mohammad, A.M. Som, M.S. Takriff, Design of a tubular ceramic membrane for gas separation in a PEMFC system, Fuel Cells 3 (4) (2003) 189–198.
[6] W.J. Koros, R. Mahajan, Pushing the limits on possibilities for large scale gas separation: which strategies? J. Membr. Sci. 175 (2) (2000) 181–196.
[7] B. Charbonnier, C. Laurent, G. Blanc, O. Valfort, D. Marchat, Porous bioceramics produced by impregnation of 3D-printed wax mold: ceramic architectural control and process limitations, Adv. Eng. Mater. 18 (10) (2016) 1728–1737.
[8] N. Tsuji, M. Yoshikawa, T. Toda, H. Machida, H. Ohgushi, Comparison of hard tissue formation in two porous hydroxyapatite scaffolds treated with hyaluronic acid sodium salt, Key Eng. Mater. 284–286 (2005) 961–964.
[9] D.S.A. Mahmod, A.A. Khan, M.A. Munot, N. Glandut, J.C. Labbe, Laser surface treatment of porous ceramic substrate for application in solid oxide fuel cells, IOP Conf. Ser. Mater. Sci. Eng. 146 (1) (2016) 012002.
[10] N. Hedayat, Y. Du, H. Ilkhani, Review on fabrication techniques for porous electrodes of solid oxide fuel cells by sacrificial template methods, Renew. Sustain. Energy Rev. 77 (2017) 1221–1239.
[11] A. Julbe, D. Farrusseng, C. Guizard, Porous ceramic membranes for catalytic reactors — overview and new ideas, J. Membr. Sci. 181 (1) (2001) 3–20.
[12] L. Kiwi-Minsker, A. Renken, Microstructured reactors for catalytic reactions, Catal. Today 110 (1–2) (2005) 2–14.
[13] V.R. Salvini, A.P. Luz, V.C. Pandolfelli, High temperature Al_2O_3-CA_6 insulating foamed ceramics: processing and properties, Interceram 61 (6) (2012) 335–339.
[14] S. Jiang, P. Liu, X. Zhang, L. Zhang, Q. Li, J. Yao, Y. Zeng, Q. Wang, G. Zhang, Enhanced pyroelectric properties of porous $Ba_{0.6}7Sr_{0.33}TiO_3$ ceramics fabricated with carbon nanotubes, J. Alloys Compd. 636 (2015) 93–96.
[15] G. Zhang, S. Jiang, Y. Zeng, Y. Zhang, Q. Zhang, Y. Yu, High pyroelectric properties of porous $Ba_{0.6}7Sr_{0.33}TiO_3$for uncooled infrared detectors, J. Am. Ceram. Soc. 92 (12) (2009) 3132–3134.
[16] G. Zhang, S. Jiang, Y. Zeng, Y. Zhang, Q. Zhang, Y. Yu, The modified model of the dielectric characteristics for porous $Ba_{0.6}Sr_{0.4}TiO_3$ ceramics, J. Appl. Phys. 106 (3) (2009) 034110.
[17] J.-F. Yang, G.-J. Zhang, T. Ohji, Porosity and microstructure control of porous ceramics by partial hot pressing, J. Mater. Res. 16 (07) (2011) 1916–1918.
[18] E.P. Simonenko, A.V. Derbenev, N.P. Simonenko, E.K. Papynov, V.Y. Maiorov, E.A. Gridasova, V.A. Avramenko, V.G. Sevastyanov, N.T. Kuznetsov, Production of porous ceramic materials using nanodisperse SiC powder, Rus. J. Inorg. Chem. 62 (7) (2017) 863–869.
[19] K. Kamitani, T. Hyodo, Y. Shimizu, M. Egashira, Fabrication of highly porous alumina-based ceramics with connected spaces by employing PMMA microspheres as a template, Adv. Mater. Sci. Eng. 2009 (2009) 1–9.
[20] D. Brouczek, T. Konegger, Open-porous silicon nitride-based ceramics in tubular geometry obtained by slip-casting and gelcasting, Adv. Eng. Mater. (2017) 1700434.
[21] C.-H. Chen, K. Takita, S. Ishiguro, S. Honda, H. Awaji, Fabrication on porous alumina tube by centrifugal molding, J. Eur. Ceram. Soc. 25 (14) (2005) 3257–3264.
[22] O. Bălţătescu, M. Axinte, G. Barbu, V. Manole, New approach for porous materials obtaining using centrifugal casting, IOP Conf. Ser. Mater. Sci. Eng. 95 (2015) 012018.
[23] M. Chai, M. Machida, K. Eguchi, H. Arai, Preparation and characterization of sol-gel derived microporous membranes with high thermal stability, J. Membr. Sci. 96 (3) (1994) 205–212.
[24] M. Othman, H. Mukhtar, Review on development of ceramic membrane from sol-gel route: parameters affecting characteristics of the membrane, IIUM Eng. J. 1 (2) (2000).
[25] Y. Grebenyuk, H.X. Zhang, M. Wilhelm, K. Rezwan, M.E. Dreyer, Wicking into porous polymer-derived ceramic monoliths fabricated by freeze-casting, J. Eur. Ceram. Soc. 37 (5) (2017) 1993–2000.
[26] R. Zhang, Q. Qu, B. Han, B. Wang, A novel silica aerogel/porous Y_2SiO_5 ceramics with low thermal conductivity and enhanced mechanical properties prepared by freeze casting and impregnation, Mater. Lett. 175 (2016) 219–222.
[27] V. Sciamanna, B. Nait-Ali, M. Gonon, Mechanical properties and thermal conductivity of porous alumina ceramics obtained from particle stabilized foams, Ceram. Int. 41 (2) (2015) 2599–2606.
[28] X. Deng, J. Wang, J. Liu, H. Zhang, L. Han, S. Zhang, Low cost foam-gelcasting preparation and characterization of porous magnesium aluminate spinel ($MgAl_2O_4$) ceramics, Ceram. Int. 42 (16) (2016) 18215–18222.
[29] R. Vinoth Kumar, A. Kumar Ghoshal, G. Pugazhenthi, Elaboration of novel tubular ceramic membrane from inexpensive raw materials by extrusion method and its performance in microfiltration of synthetic oily wastewater treatment, J. Membr. Sci. 490 (2015) 92–102.
[30] P. Fan, K. Zhen, Z. Zan, Z. Chao, Z. Jian, J. Yun, Preparation and development of porous ceramic membrane supports fabricated by extrusion technique, Chem. Eng. Trans. 55 (2016) 277–282.
[31] R.H.R. Castro, D. Gouvêa, F. Wakai, Sintering and nanostability: the thermodynamic perspective, J. Am. Ceram. Soc. 99 (4) (2016) 1105–1121.
[32] S. Das, V. Jayaraman, SnO_2: a comprehensive review on structures and gas sensors, Prog. Mater. Sci. 66 (2014) 112–255.
[33] S. Chappel, A. Zaban, Nanoporous SnO_2 electrodes for dye-sensitized solar cells: improved cell performance by the synthesis of 18 nm SnO_2 colloids, Sol. Energ. Mater. Sol. Cells 71 (2) (2002) 141–152.
[34] Q.-r. Zhao, Controllable synthesis and catalytic activity of SnO_2 nanostructures at room temperature, Trans. Nonferrous Metals Soc. China 19 (5) (2009) 1227–1231.
[35] A.B. Glot, R. Bulpett, A.I. Ivon, P.M. Gallegos-Acevedo, Electrical properties of SnO_2 ceramics for low voltage varistors, Physica B Condens. Matter 457 (2015) 108–112.
[36] B. Huang, X. Li, Y. Pei, S. Li, X. Cao, R.C. Masse, G. Cao, Novel carbon-encapsulated porous SnO_2 anode for lithium-ion batteries with much improved cyclic stability, Small 12 (14) (2016) 1945–1955.
[37] J.A. Varela, L.A. Perazolli, J.A. Cerri, E.R. Leite, E. Longo, Sintering of tin oxide and its applications in electronics and processing of high purity optical glasses, Cerâmica 47 (2001) 117–123.
[38] P.R. Bueno, J.A. Varela, E. Longo, SnO_2, ZnO and related polycrystalline compound semiconductors: an overview and review on the voltage-dependent resistance (non-ohmic) feature, J. Eur. Ceram. Soc. 28 (3) (2008) 505–529.
[39] J.A. Cerri, E.R. Leite, D. Gouvêa, E. Longo, J.A. Varela, Effect of cobalt(II) oxide and manganese(IV) oxide on sintering of tin(IV) oxide, J. Am. Ceram. Soc. 79 (3) (1996) 799–804.
[40] https://imagej.nih.gov/ij/ (Accessed 31 January 2017).
[41] R.F. Marcomini, D.M.P.F.d. Souza, Caracterização microestrutural de materiais cerâmicos utilizando o programa de processamento digital de imagens Image J, Cerâmica 57 (2011) 100–105.
[42] A.F. Ismail, L.I.B. David, A review on the latest development of carbon membranes for gas separation, J. Membr. Sci. 193 (1) (2001) 1–18.
[43] P. Pandey, R.S. Chauhan, Membranes for gas separation, Prog. Polym. Sci. 26 (6) (2001) 853–893.
[44] M.N. Rahaman, Ceramic Processing and Sintering, 2nd ed., Taylor & Francis, New York, NY, 2003.
[45] G. Elssner, H. Hoven, G. Kiessler, P. Wellner, Ceramics and Ceramic Composites: Materialographic Preparation, 1st ed., Elsevier Science, New York, NY, 1999.
[46] S. Canovic, T. Jonsson, M. Halvarsson, Grain contrast imaging in FIB and SEM, J. Phys. Conf. Ser. 126 (2008) 012054.
[47] O.A. Lukianova, V.V. Sirota, Dielectric properties of silicon nitride ceramics produced by free sintering, Ceram. Int. 43 (11) (2017) 8284–8288.
[48] K. Negita, Effective sintering aids for silicon carbide ceramics: reactivities of silicon carbide with various additives, J. Am. Ceram. Soc. 69 (12) (1986) C-308–C310.
[49] S.S. Rehman, W. Ji, S.A. Khan, Z. Fu, F. Zhang, Microstructure and mechanical properties of B_4C densified by spark plasma sintering with Si as a sintering aid, Ceram. Int. 41 (1) (2015) 1903–1906.
[50] K. Watari, H.J. Hwang, M. Toriyama, S. Kanzaki, Effective sintering aids for low-temperature sintering of AlN ceramics, J. Mater. Res. 14 (04) (2011) 1409–1417.